2012

Performance of a Compact Absorption Heat Pump Containing Microchannel Absorber Components

Ward E. TeGrotenhuis
ward.tegrotenhuis@pnnl.gov

Dustin D. Caldwell

Paul H. Humble

Dale A. King

Shankar Krishnan

Performance of a Compact Absorption Heat Pump Containing Microchannel Absorber Components

Ward TE GROTENHUIS [1,2]*, Dustin CALDWELL [2], Paul HUMBLE [2], Dale KING [2], Shankar KRISHNAN [1,2] and Jair LIZARAZO-ADARME [1,2]

[1] Microproducts Breakthrough Institute,
Corvallis, Oregon, USA
509-372-4049, ward.tegrotenhuis@pnnl.gov

[2] Pacific Northwest National Laboratory, Thermal and Reaction Systems,
Richland, Washington, USA

* Corresponding Author

ABSTRACT

Novel microchannel absorbers have been scaled-up and incorporated into a 5-kW-scale ammonia-water absorption heat pump. The planar microchannel absorbers operate with thin wick structures to enhance mass transfer in the absorption channels which are interleaved with microchannel heat exchange layers. The resulting rapid heat and mass transfer facilitates significant size reduction in the absorber and consequently the overall heat pump system. Based on the 5-kW-scale system design, up to 50% size reduction relative to current commercial equipment is projected. The microwick absorber technology is described and measured performance data are provided for proof-of-concept single-channel devices up to multi-channel devices tested in a 300 Watt breadboard. The design of 5 kW system includes a unique configuration of components to enable high COP exceeding 0.5 at military conditions of 50°C ambient temperature. The 5 kW system design is discussed and performance data are provided from initial laboratory testing. Cost of the microwick components is expected to be higher than conventional equipment. Volume sensitive cost estimation models are described that have been used to predict the manufactured costs of the microwick absorber devices. The resulting cost-volume curves provide insights into the potential trade-off between size and system cost.

1. INTRODUCTION

Heat-activated cooling technologies, such as absorption heat pumps, facilitate use of alternative energy sources for air conditioning, refrigeration, and other cooling applications. Possible heat sources include solar thermal, burning natural gas and other fuels, waste heat, or from within integrated systems, such as combined cooling, heating, and power (CCHP) and tri-generation systems (Deng, Wang et al. 2011). For example, waste heat from a solid oxide fuel cell that runs at over 600°C can be used to operate an absorption cooling system to supply shipboard HVAC (Tse, Wilkins et al. 2011). Integrated energy systems can lead to substantial fuel savings, which for military applications, such as mobile command centers and forward operating bases, represents significant cost savings and lessens the endangerment of lives in transporting fuel. System studies have indicated that operating an absorption heat pump using heat recovered from exhaust of a Tactical Quiet Generator could save as much as 44% of the fuel cost over a vapor compression system using generated power. However, mobile applications require small, lightweight systems, and available systems are generally impractical for these uses. In addition, smaller, lighter, and lower-cost components will facilitate the adoption of the complex, multi-effect systems that are necessary for achieving high energy efficiency (Garimella, Determan et al. 2011).

An absorption heat pump cycle is depicted in Figure 1 for ammonia-water working fluid. The refrigerant loop contains a condenser, a throttle valve, and an evaporator just like in conventional vapor compression systems.

However, instead of a mechanical compressor that is driven with electrical power, a thermochemical compressor using high temperature heat is used to produce high pressure. The ammonia is absorbed into a water solution at low pressure and temperature while the heat of absorption is rejected to a coolant. The solution is pumped to high pressure before being preheated first in a recuperative heat exchanger and then in a desorber, which produces ammonia and a small amount of water at high pressure. The solution is then cooled and expanded before returning to the absorber. The rectifier removes water from the refrigerant stream. With the mechanical compressor eliminated, the electrical demand is reduced significantly to only parasitic loads for pumps and blowers.

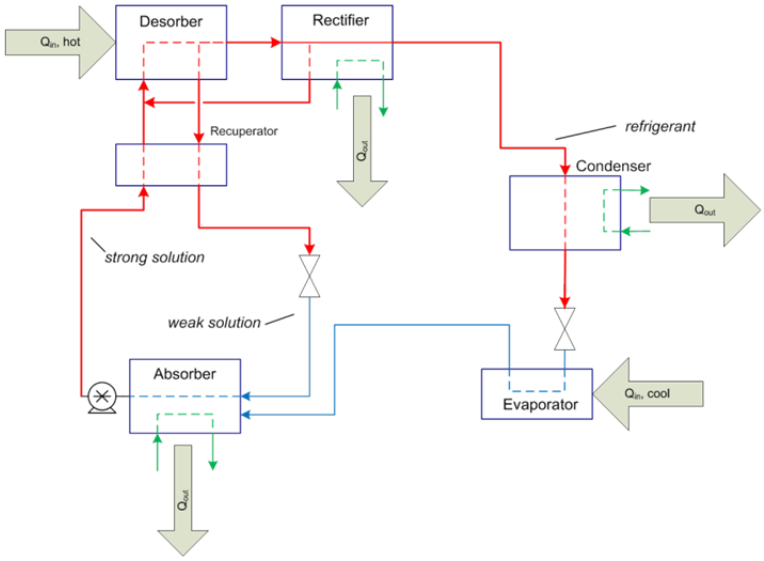

Figure 1. Absorption heat pump schematic with red and blue lines indicating high and low pressures, respectively.

The components in Figure 1 that involve both liquids and gases are the absorber, desorber, and rectifier. Of these, the most challenging unit operation is the absorber, because it is generally limited by both heat and mass transfer. As pointed out by Srikhirin et al. (2001), the size and performance of the absorber can be severely limited by equilibrium, often leading to 2-5 times the minimum required solution flow rate. The conventional approach is falling film absorbers (Killion and Garimella 2001; Killion and Garimella 2003; Kwon and Jeong 2004), and several groups have developed alternative approaches to improve performance and reduce size and weight. Lee et al. (2002), Merrill and Perez-Blanco (1997), and others have investigated bubble-plate absorbers, for example. Heat transfer resistance on the cold side can also limit performance, and Garimella et al. (2011) utilize banks of microchannel tubes to improve coolant-side heat transfer while also enhancing absorption heat and mass transfer. Wang et al. (2007) analyzed the relative importance of air-cooled absorbers versus using hydronic loops. The work described here is to develop and demonstrate compact absorbers using patented microwick technology (TeGrotenhuis, Wegeng et al. 2003; TeGrotenhuis and Stenkamp 2005; TeGrotenhuis and Stenkamp 2006).

2. MICROWICK ABSORPTION

2.1 Microwick Concept

The use of thin wicks for gas-liquid processing in microchannels has been successfully applied to phase separation (TeGrotenhuis, Stenkamp et al. 2005), partial condensation with phase separation (TeGrotenhuis and Stenkamp 2003), and distillation (Huang, King et al. 2008). The technology has also been demonstrated to work effectively in reduced-gravity on NASA's KC-135 zero gravity aircraft (TeGrotenhuis and Stenkamp 2003; TeGrotenhuis, Stenkamp et al. 2005). The concept of a thin-wick absorber is illustrated by the schematic of Figure 2. A planar wick that is 0.1 to 0.5 mm thick is located in a small channel with a plenum adjacent to the wick. When a gas and liquid are introduced into the channel and the liquid wets the wick, the liquid will preferentially segregate and flow through the wick. With the liquid confined to and flowing through the wick, the characteristic length-scale for mass transfer is the thickness of the wick. In addition, because the heat of absorption is produced at the gas-liquid interface, heat is also transported through the wick thickness. Therefore, both heat and mass transfer rates on the absorption side scale inversely with the thickness of the wick.

Heat exchange channels are incorporated in a stacked-plate architecture, which is also depicted in Figure 2, in order to remove the heat of absorption. Scale-up is accomplished by alternately stacking absorption channels and heat exchange channels, resulting in an interleaved structure. By using microchannels for both the absorption and heat exchanger channels, very high surface area to volume ratios are achieved that contribute to reducing size and weight. While Figure 2 shows a single wick in the absorbing channel, wicks are actually placed on both walls of the absorbing channels to maximize wick flow area and mass transfer area, and to minimize the overall heat transfer resistance.

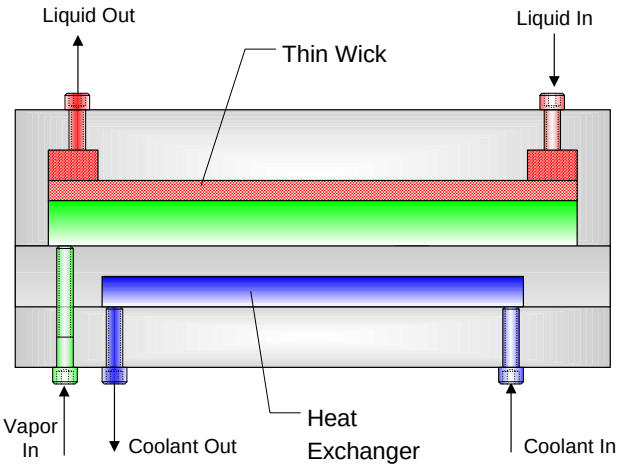

Figure 2. Schematic of the micowick absorber concept.

The mass transfer performance of a wicking absorber is assessed using two dimensionless groups, an overall mean Sherwood number and a mass transfer Peclet number. The Sherwood number is calculated by

$$Sh_{om} = \frac{k_{om}\, h}{D_{AB}} \tag{1}$$

where h is the characteristic length-scale for mass transfer, D_{AB} is the binary diffusion coefficient, and k_{om} is the overall mean mass transfer coefficient, defined by

$$k_{om} = j \,/\, lmcd \tag{2}$$

where j is the average mass flux or total mass uptake divided by mass transfer area, and *lmcd* is the log-mean of the inlet and outlet concentration driving forces. Assuming mass transfer resistance is dominated by the liquid phase, *lmcd* is calculated assuming the liquid concentration at the gas-liquid interface is in equilibrium with ammonia vapor at a given temperature and pressure. The concentration driving force is the difference between the calculated equilibrium interface concentration and the bulk measured concentration.

The residence time of the solution is characterized by the inverse mass transfer Peclet number, calculated by

$$\frac{1}{Pe} = \frac{D_{AB}}{\bar{v}\, h} \tag{3}$$

where $\bar{v}$ is the average liquid velocity. The inverse Peclet number indicates the expected mass transfer effectiveness; 1/Pe<<1 indicates insufficient residence time for mass transfer, while equilibrium is approached as 1/Pe>>1. Approach to equilibrium can be expressed in terms of stream temperature as

$$\Delta T_{eq} = \bar{T} - T_{sat}\left(P_v, \bar{c}\right) \tag{4}$$

where $\bar{T}$ is the average solution temperature, and T_{sat} is the saturation temperature at a given vapor pressure P_v and average concentration $\bar{c}$. Close approach to equilibrium improves the performance of an absorption cycle heat pump by enabling lower solution recirculation ratios—the ratio of solution mass flow to refrigerant mass flow.

2.1 Proof-of-Concept to Breadboard Demonstration

Early proof-of-concept data were acquired using a single-channel device which is shown in the left picture in Figure 3. This device consisted of four layers that were bolted together with gaskets to form a single absorption channel surrounded by two water-cooled heat transfer channels. The ability to disassemble the device facilitated testing of various wick structures. The device was successful in demonstrating the microwick absorption concept, and achieved Sherwood numbers between 0.45 and 0.6 in the range of 1/Pe from 0.9 to 1.6 (TeGrotenhuis, Stenkamp et al. 2005).

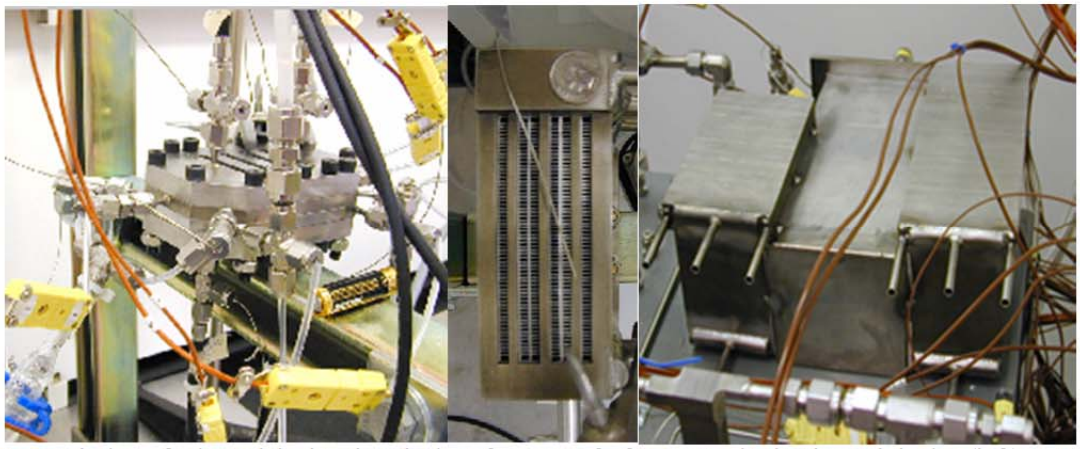

Figure 3. Evolution of microwick absorber devices from proof-of-concept single-channel device (left) to 3-channel air-cooled device (center), to 12- and 18-channel devices for system testing.

The next step in developing the microwick absorber was the 3-channel, cross-flow air-cooled device shown in the center picture of Figure 3. The picture was taken from above, and the air heat exchangers are visible, which are press-fit aluminum elements in a stainless-steel laminate construction. The wicks are on edge within the walls between the air heat exchangers. This configuration is referred to as side-flow, and the device was also tested in a vertical orientation, where the solution flows downward. Results from the 3-channel device are shown in Figure 4 that are consistent with data obtained from the single-channel device.

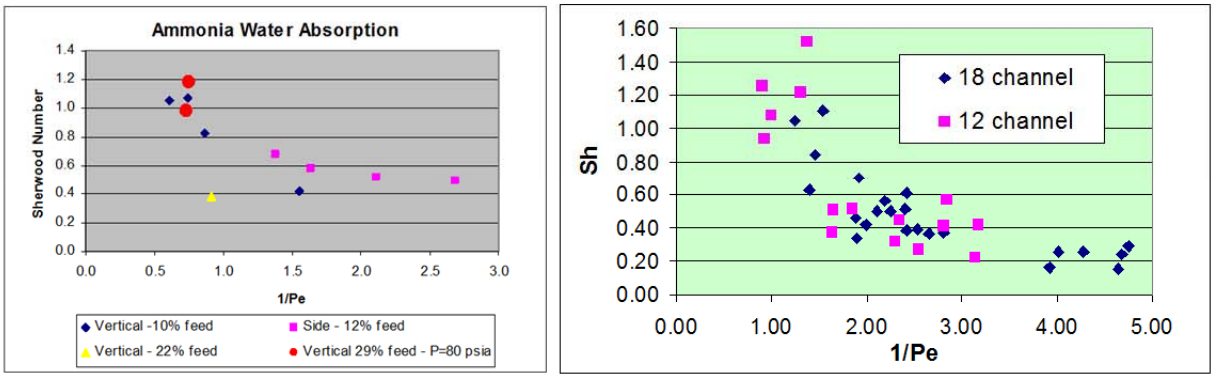

Figure 4. Consistent performance in scaling-up from 3-channel pre-prototype device (left) and 12- and 18-channel devices used for a breadboard demonstration.

Subsequent to verify that performance could be reproduced in a multi-channel pre-prototype device, the air-cooled design was scaled up to 12-channel and 18-channel devices for testing within a 500 Watt breadboard system. The right picture in Figure 3 shows the 12-channel device on the left and the 18-channel device on the right attached to an air plenum. These devices were only tested in vertical, down-flow configuration. Results from the larger devices are included in Figure 4 and show that the mass transfer performance remained consistent in scaling up.

3. SCALE-UP TO 5 kW SYSTEM

The next step in developing the microwick absorber technology was scale-up and testing in a 5.3 kW demonstration system. A P&ID is provided in Figure 5 of the system, which consisted of several microchannel components as well as off-the-shelf (OTS) purchased components. The OTS evaporator produces chilled water that is sent to a separate 'cold box' in a split system. Also apparent from Figure 5 is the use of a hydronic loop (black lines) for cooling the microchannel absorbers and OTS condensers. For the purpose of demonstration, heated oil is supplied to the desorber from an external electric oil heater, which would be integrated with a heat source when deployed for a specific application.

One of the advantages of microchannel process technology (MPT) is the modularity that makes it convenient to integrate additional components with minimal increase in size and weight. Several MPT components are included in the 5.3 kW demonstration system in addition to the MPT absorber and MPT recuperator in order to improve overall system efficiency and take advantage of thermodynamic driving forces. The solution loop includes MPT pre-cooler, pre-mixer, and pre-absorber. The pre-cooler is a simple MPT heat exchanger that cools the weak solution up stream of the throttle valve to preclude flashing ammonia and to maximize the water temperature in the hydronic loop and reduce radiator size. The pre-mixer is a microwick device without heat exchange channels for cooling, and serves the purpose of adiabatically mixing ammonia and weak solution. By maximizing the temperature of the solution entering the pre-absorber, additional heat can be recuperated into the strong solution in the pre-absorber for higher energy efficiency. Additional efficiency gains are obtained from the condensate precooler, a small MPT heat exchanger, which cools the refrigerant prior to expansion using additional cooling capacity in the refrigerant exiting the evaporator. Adding the MPT microwick rectifier, there are a total of 7 MPT devices in the system, of which 4 are microwick devices. The system design projects 5.3 kW of evaporator duty at a projected gross COP of 0.63 at military conditions of 50°C outside temperature.

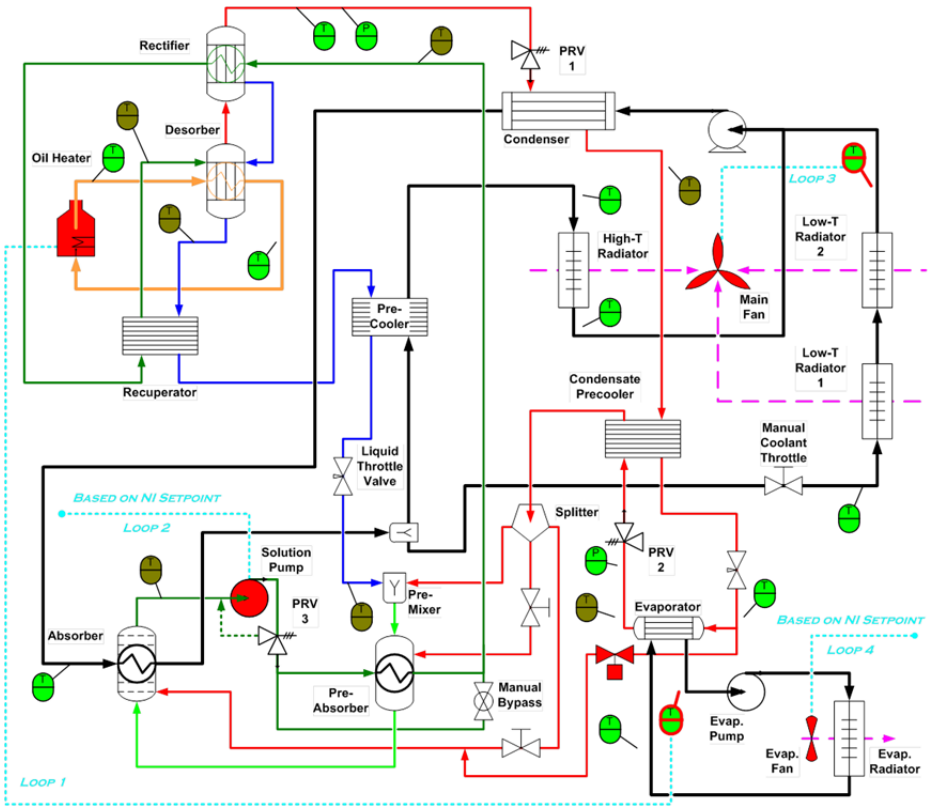

Figure 5. Piping and instrumentation diagram of the 5.3 kW ammonia-water absorption heat pump system.

The packaged 'hot box' of the demonstration system is shown in Figure 6A. The overall dimensions are 0.66 m width by 0.72 m depth by 0.64 m height to the top of the fan. The configuration of the MPT components and the

customized desorber is shown in Figure 6B, and the absorbers, which are located toward the lower back in Figure 6B, are the largest MPT component in the system. Two absorbers of the size indicated by Figure 6C are oriented in down-flow in the system. When the system is scaled-up to a full 5-ton system, the size and weight are both projected to be approximately 50% of a commercial Robur 5-ton system, which is the smallest commercial system that could be identified.

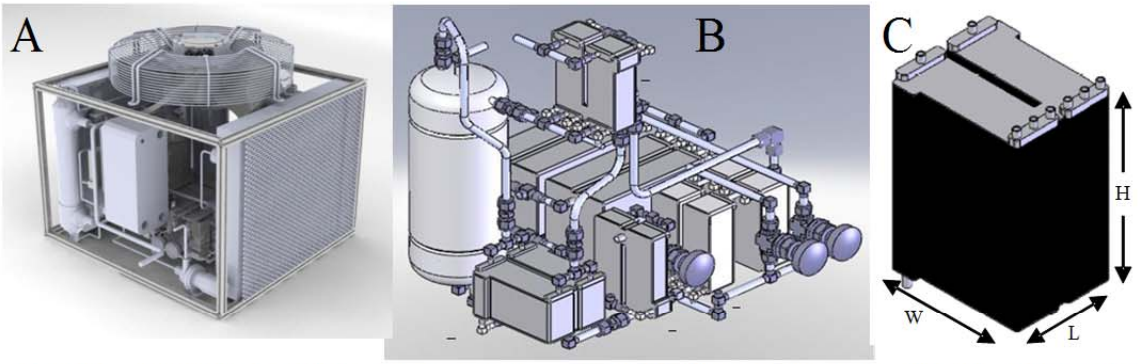

Figure 6. Ammonia absorption cycle heat pump system (A) utilizing MPT devices (B). The 5 kW system requires two absorbers (C) each with external dimensions of approximately 15 cm (W) x 15 cm (L) x 25 cm (H).

The architecture of the absorber device (MPT) is based on a stacked-shim fabrication process in which shims are first patterned and then bonded into a monolithic stack as described by Leith et al. (2010). Two machined end-plates are joined to either end of the device to provide structural strength and attachment of fluidic interconnects. The service environment of the absorber requires mechanical strength at elevated temperature with a corrosive fluid, so austenitic 316 stainless steel is used for both shims and end-plates in all the MPT devices.

Shakedown and testing of the 5.3 kW system is underway and is progressing toward the target of 5.3 kW duty and a gross COP of 0.62 at military conditions of 50°C outside temperature. To date, the system has produced slightly less than 50% of the expected cooling duty at a gross COP of 0.47.

One of the discoveries made during early testing was excessive cooling of the refrigerant stream in the rectifier resulting in too much condensation and recycle back to the desorber and causing loss of cooling capacity. Consequently, a bypass was installed, which is not shown in Figure 5, to divert strong solution around the rectifier in order to facilitate control of the refrigerant exit temperature. The increase in cooling capacity obtained by raising the refrigerant temperature from 45°C to 67°C and then to 72°C is shown in Figure 7. In addition, the COP increased from about 0.3 to over 0.4.

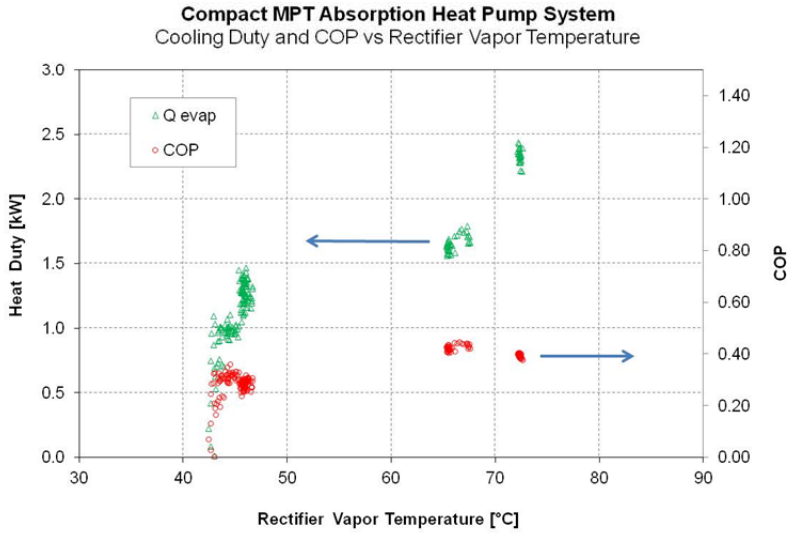

Figure 7. Cooling duty and COP as a function of rectifier vapor temperature.

Figure 8 illustrates the effects of both desorber temperature and rectifier bypass on COP and cooling duty of the compact absorption heat pump. As expected, with all other parameters constant, higher oil temperature increases the cooling duty for a given rectifier bypass valve position. The higher cooling duty and COP observed at higher rectifier bypass is consistent with the results in Figure 7.

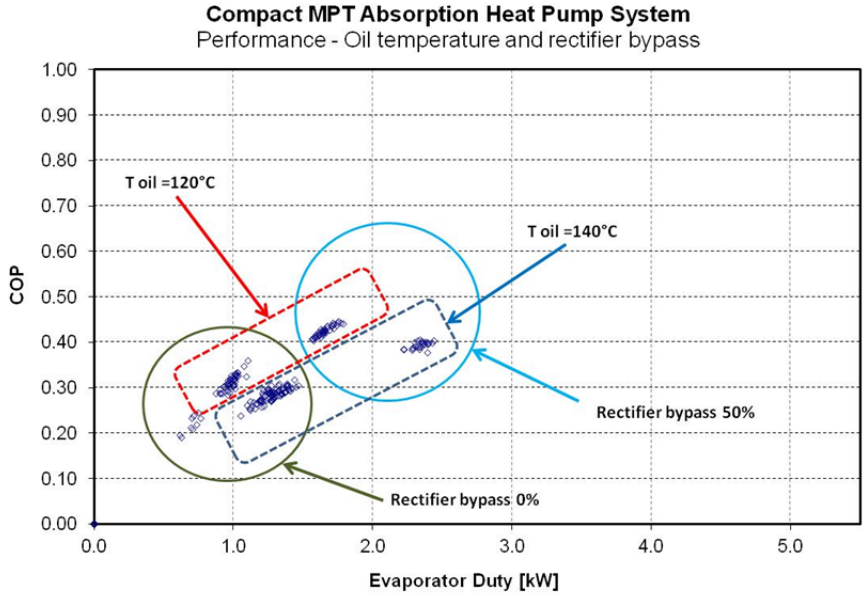

Figure 8. Oil temperature and rectifier bypass effect on COP and evaporator duty of compact MPT Absorption Heat Pump. Oil temperature = 120 and 140 °C and rectifier bypass = 0 and 50%.

Future testing includes raising reject temperature to a simulated 49°C by adjusting fan speeds and flow rate of the hydronic cooling loops; increase desorber operating temperature (oil temperature); and determine the effect of total charge and charge concentration on the performance of the compact MPT absorption heat pump.

4. COST OF MANUFACTURING

To move from technology demonstration to market entry and commercialization, requires an understanding of the manufacturing processes and associated cost structures necessary to fabricate components in production volumes. Recent work at the MBI has focused on developing volume-sensitive cost estimation models for predicting the manufacturing costs of MPT devices fabricated using a range of processing technologies. The total manufacturing cost of MPT is broken down into a number of cost elements associated with each step in the production process. Typical cost elements include capital equipment, labor, direct materials, indirect materials, energy/utilities, facilities and maintenance. Variation in each cost element is estimated through creation of functional relationships that quantify the impact of manufacturing variables (*e.g.* production volume, equipment through-put, labor and loading rates, electricity cost, etc.) on each cost element. Each cost element is estimated separately for each production step and summed to establish overall manufacturing cost for cost element and for production step. The output from the process-based model is an estimate of cost of goods sold (COGS); typical overhead cost contributors such as sales and marketing, R&D, administration, management, profit and taxes are not included.

Application of the process-based cost modeling methodology to manufacturing of a device such as the absorber shown in Figure 6 can be used to illustrate the relative contribution of design, materials and fabrication process choice on final device cost. The process-based costs models are used to develop an understanding of the economic trade-offs between candidate processes and are utilized in a design for manufacturing approach to MPT device development. In this paper we present results and analysis of the cost modeling effort to date and apply the methodology in a case study of the heat pump absorber device designed, built and tested by Pacific Northwest National Laboratory. The process-based cost model is used here to identify primary cost drivers in the manufacture

of the ammonia absorber device and to illustrate the interaction of design and COGS across a range of production volumes. A number of fabrication processes have been used at MBI to build demonstration devices. The most-widely used process steps, is especially well-suited for fabricating metallic-based MPT devices at low (prototype) volumes.

On this "default" manufacturing process flow described by Paul (2006), photochemical machining (PCM) is used to pattern shims, diffusion bonding for joining of the shim stack, electro-discharge machining (EDM) for final device perimeter shaping and CNC milling to define fluidic interconnects. These fabrication processes of these prototypes have been performed by third party contract manufacturers and the cost of device fabrication is very likely not representative of that which could be achieved using a dedicated production line as is assumed with the proposed cost model. The default process of the process-based cost model is used to predict manufacturing costs of the absorber at anticipated market demand of 100, 1,000 and 10,000 absorbers/year. In a manufacturing environment, the cost of raw materials in practice generally decreases as volumes increase as a result of high-volume price discounts from sheet metal suppliers. In the current model analysis, however, the price per unit mass of stainless steel sheet stock remains fairly constant over the device production range investigated.

Figures 9 and 10 illustrate the manufacturing cost breakdown of MPT absorption heat pump system and MPT absorber by component and process step respectively. While the total fabrication cost of the heat pump system decreases from $66,600 to $5,700 by increasing the production volume from 100 to 10,000 systems/year, the cost contribution of MPT absorber seems to be the higher cost regardless of production volume. This suggests significant opportunities for cost reduction during patterning process step. For example, shim patterning can be performed using a number of other fabrication processes including electrochemical machining (ECM), stamping (piercing or coining), laser cutting and abrasive water jet cutting. Direct comparison of the cost associated with each of these processes for the patterning of specific shim architectures will illustrate which candidate processes are likely to be the most economical in production. Because of characteristic limitations of each candidate pattern process, alternative shim designs may be needed to be considered to enable lower fabrication cost of MPT devices.

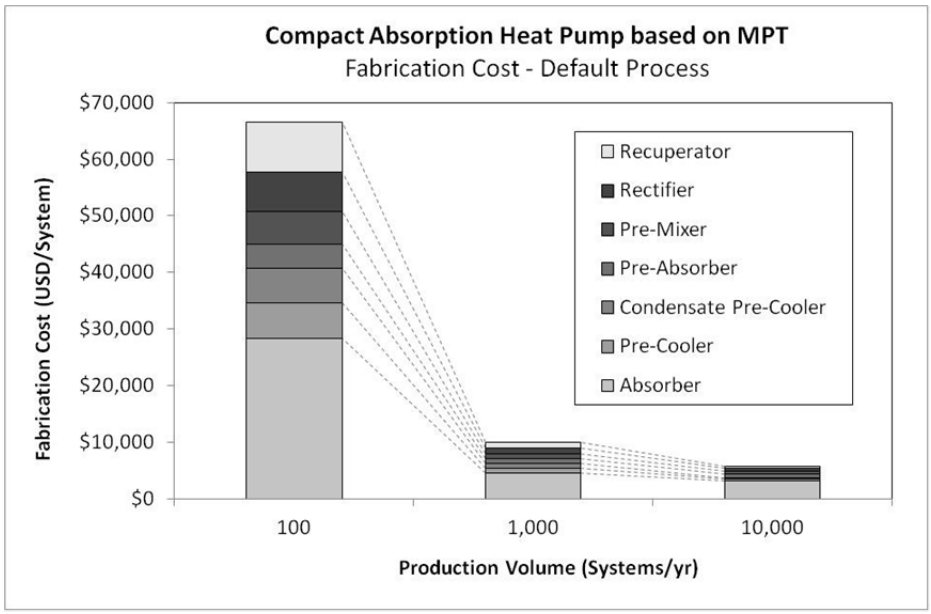

Figure 9. Manufacturing cost breakdown by components of MPT absorption heat pump system at 100, 1,000 and 10,000 units/year production.

As illustrated on **Figure** , across all the production volumes, PCM shim patterning and diffusion bonding process present the higher contribution to the manufacturing cost of the MPT absorber as well as for the other MPT devices (no showed here). Model simulations predict that PCM costs actually increase as a fraction of the total cost with increased volume production even while decreasing on a unit COGS basis.

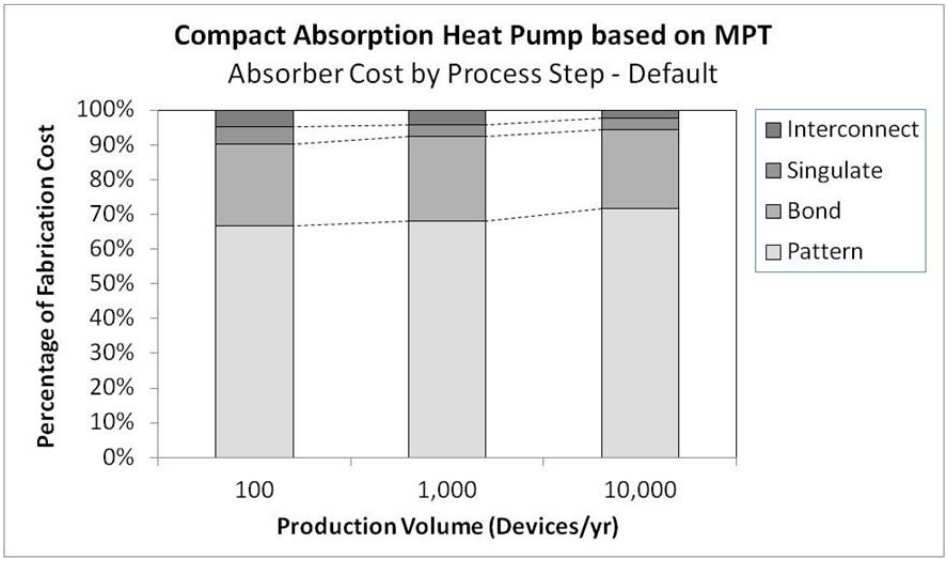

Figure 10. Manufacturing cost breakdown by process step of MPT absorber at 100, 1,000 and 10,000 units/year production.

The rate of cost reduction with volume predicted for the PCM process is characteristic of a manufacturing process line designed for a maximum capacity of 40,000 m^2/yr. At low production, the production line is under-utilized and fixed costs associated with capital and labor is allocated to a small number of parts, increasing the base unit cost. As production volumes increases, both capital and labor utilization improve and unit COGS decrease. When the direct material cost (*i.e.* 316 SS shim stock) is removed from the analysis, Leith et al. (2010) predicts a decrease in manufacturing cost to approximately $1.25 per shim. The proposed cost model can be used further to explore the cost drivers inherent in the PCM process and to evaluate the financial viability of this option as a candidate fabrication option in an MPT production environment.

5. CONCLUSIONS

A new microwick technology has been presented that uses capillary forces within microchannel devices to reduce size and weight of the absorber and other components of absorption heat pumps. The technology has been successfully scaled up from a single-channel proof-of-concept device to components for a 5.3 kW compact absorption heat pump system with very consistent performance. The utility of microchannel technology in achieving high levels of thermal integration through additional compact components has been illustrated in the 5.3 kW system, which has a projected COP of 0.63 in a single-effect system operating at 50°C reject temperature. Testing is underway to achieve performance targets, and current status is 50% of design cooling capacity at 0.47 COP.

System cost is a key factor in deploying the technology for both military and commercial applications. Identification of cost drivers is a critical enabler in effectively prioritizing the fabrication processes that gives the highest probability for commercial success. Cost model sensitivity analyses has be used to determine areas of technical and/or financial risk and are a useful tool in developing more sophisticated economic assessments; for example supporting a “make vs. buy” decision in manufacturing production.

REFERENCES

Deng, J., R. Z. Wang, et al. (2011). "A review of thermally activated cooling technologies for combined cooling, heating and power systems." Progress in Energy and Combustion Science **37**(2): 172-203.

Garimella, S., M. D. Determan, et al. (2011). "Microchannel component technology for system-wide application in ammonia/water absorption heat pumps." International Journal of Refrigeration **34**(5): 1184-1196.

Huang, X., D. A. King, et al. (2008). "Hydrodesulfurization of JP-8 fuel and its microchannel distillate using steam reformate." Catalysis Today **136**(3–4): 291-300.

Killion, J. D. and S. Garimella (2001). "A critical review of models of coupled heat and mass transfer in falling-film absorption." International Journal of Refrigeration **24**(8): 755-797.

Killion, J. D. and S. Garimella (2003). "Gravity-driven flow of liquid films and droplets in horizontal tube banks." International Journal of Refrigeration **26**(5): 516-526.

Kwon, K. and S. Jeong (2004). "Effect of vapor flow on the falling-film heat and mass transfer of the ammonia/water absorber." International Journal of Refrigeration **27**(8): 955-964.

Lee, K. B., B. H. Chun, et al. (2002). "Experimental analysis of bubble mode in a plate-type absorber." Chemical Engineering Science **57**(11): 1923-1929.

Leith, S. D., D. A. King, et al. (2010). Paper 335d: Toward Low-Cost Fabrication of Microchannel Process Technologies - Cost Modeling for Manufacturing Development. 2010 AIChE Annual Meeting, Salt Lake City, UT.

Merrill, T. L. and H. Perez-Blanco (1997). "Combined heat and mass transfer during bubble absorption in binary solutions." International Journal of Heat and Mass Transfer **40**(3): 589-603.

Paul, B. K. (2006). Micro energy and chemical systems and multi-scale fabrication. Micromanufacturing and Nanotechnology. N. P. Mahalik. Berlin, Germany, Springer-Verlag**:** 323-352.

Srikhirin, P., S. Aphornratana, et al. (2001). "A Review of Absorption Refrigeration Technologies." Renewable and Sustainable Energy Reviews **5**: 343-372.

TeGrotenhuis, W. E. and V. S. Stenkamp (2003). Testing of a Microchannel Partial Condenser and Phase Separator in Reduced Gravity. First International Conf. on Microchannels and Minichannels, New York, N.Y., ASME.

TeGrotenhuis, W. E. and V. S. Stenkamp (2005). Improved Conditions for Fluid Separations in Microchannels, Capillary-Driven Fluid Separations, and Laminated Devices Capable of Separating Fluids. U.S. Patent 6,875,247.

TeGrotenhuis, W. E. and V. S. Stenkamp (2006). Methods for Fluid Separations, and Devices Capable of Separating Fluids. U.S. Patent 7,051,540.

TeGrotenhuis, W. E., V. S. Stenkamp, et al. (2005). "Miniaturization of an Ammonia-Water Absorption Cycle Heat Pump using Microchannels." Int. Sorption Heat Pump Conf.

TeGrotenhuis, W. E., V. S. Stenkamp, et al. (2005). Gas-Liquid Processing in Microchannels. Microreactor Technology and Process Intensification. Y. Wang and J. D. Holladay. Washington, D.C., American Chemical Society. **914:** 360-377.

TeGrotenhuis, W. E., R. S. Wegeng, et al. (2003). Microsystem Capillary Separations. U.S. Patent 6,666,909.

Tse, L. K. C., S. Wilkins, et al. (2011). "Solid oxide fuel cell/gas turbine trigeneration system for marine applications." Journal of Power Sources **196**(6): 3149-3162.

Wang, L., G. M. Chen, et al. (2007). "Thermodynamic performance analysis of gas-fired air-cooled adiabatic absorption refrigeration systems." Applied Thermal Engineering **27**(8–9): 1642-1652.

ACKNOWLEDGEMENT

Funding for this work has been provided by the U.S. Army through the Communication-Electronics RD&E Center at Ft. Belvoir and the Natick Soldier System Center. Additional contributors include V. Susie Stenkamp, one of the original inventors and developers of the microwick technology, Steven Leith,who developed the manufacturing cost models, Don Higgins, who assembled and is operating the 5.3 kW system, and Ben Roberts, who made significant contributions to early experimental work and to the 500 kW breadboard.